ers by collagen peptides and mild skin application of retinol by multilayer structure

Jihui Jang[1], Rafia Tasnim Rahman[2], Heemuk Oh[1], Seoyoon Lee[1], Sung Yun Hong[1], Jihyun Lee[1], Chun Ho Park[1], Jun Bae Lee[1,*], Yoonsung Nam[2,*]

[1]R&I Center, COSMAX, Seongnam-si, Republic of Korea; [2]Department of Biological Sciences, KAIST, Daejeon, Republic of Korea. Email: jblee@cosmax.com (J.B.L.) and yoonsung@kaist.ac.kr (Y.N.).

1. Introduction

Lipid nanovesicles have been widely investigated as nanocarriers for drug and gene delivery owing to their favorable properties, including high biocompatibility, biodegradability, and efficient intracellular transport. Techniques such as thin film hydration followed by membrane extrusion have enabled the incorporation of both hydrophilic and hydrophobic agents into vesicular structures. In addition, high-pressure homogenization and emerging microfluidic platforms have provided scalable and tunable routes for lipid nanoparticle fabrication. Despite these advances, lipid nanovesicles are fundamentally limited by their structural instability. Because their formation relies on delicate hydrophilic–hydrophobic interactions, external stimuli such as heat, ionic strength, or pH changes can induce vesicle disruption, leakage, or aggregation, ultimately compromising their functionality and storage stability. Various approaches have been suggested to solve this problem, including the chemical crosslinking and polymerization of pre-formed lipid vesicles using polymerizable lipids, polymer/lipid hybridization, polymer coatings of lipid vesicles, and multilamellar lipid vesicles using covalent crosslinkers. Although such chemical modifications and hybridization with polymers can increase the membrane integrity and colloidal stability of lipid nanoparticles, the approaches reduce the desirable dynamic properties of lipid nanoparticles and complicate their in vivo metabolic fates. In contrast, non-covalent approaches, such as electrostatic layer-by-layer assembly using polyelectrolytes or polymer coatings, offer an alternative route for vesicle stabilization (Koo et al., 2021). Recent studies have demonstrated that specific biomolecules, such as nucleic acids, proteins, or polypeptides, can interact with charged lipid vesicles to induce phase transitions into multilamellar structures, although precise control of such interactions remains a technical challenge due to the heterogeneous nature of biomolecule surface charges.

Retinoids are a class of compounds with therapeutic and cosmetic potential due to their ability to modulate cell proliferation, collagen synthesis, and skin barrier function. Through binding to cytosolic retinoid receptors, they regulate gene expression involved in dermal regeneration and extracellular matrix remodeling. However, their clinical application is limited by chemical instability under light and heat, as well as significant irritancy, which often manifests as inflammation, erythema, and barrier disruption. These adverse effects are partly attributed to retinoid degradation products and genetic imbalance in skin barrier proteins. As a result, multiple strategies, including polymer conjugation, nano-complexation, and encapsulation in lipid-based systems, have been investigated to improve the stability and reduce the irritation profile of retinoids, while maintaining or enhancing their biological efficacy.

In this study, we propose a non-covalent stabilization strategy for retinol stabilization and delivery through the self-assembly of multilamellar collagen-lipid hybrid vesicles (MLVs) with hydrolyzed collagen peptides (HCPs) as natural, biocompatible intercalators. Cationic large unilamellar vesicles (LUVs) composed of DOTAP were prepared using the thin film hydration-extrusion method and loaded with all-trans-retinol (ATRL) within their hydrophobic bilayer domains (Rahman et al., 2024). These ATRL-loaded LUVs were then transformed into MLVs by electrostatic complexation with anionic HCPs, as schematically depicted in Figure 1. We systematically examined how HCP-to-lipid weight ratios and ionic strength influence vesicle size, surface charge, and encapsulation efficiency. Furthermore, we assessed whether the multilamellar configuration enhances retinol stability and mitigates cytotoxicity. Using artificial skin models, we compared the biological activity of ATRL delivered from unilamellar and multilamellar vesicles by measuring the expression of collagen synthesis and matrix metalloproteinase genes, providing insight into the efficacy of this bioinspired delivery system.

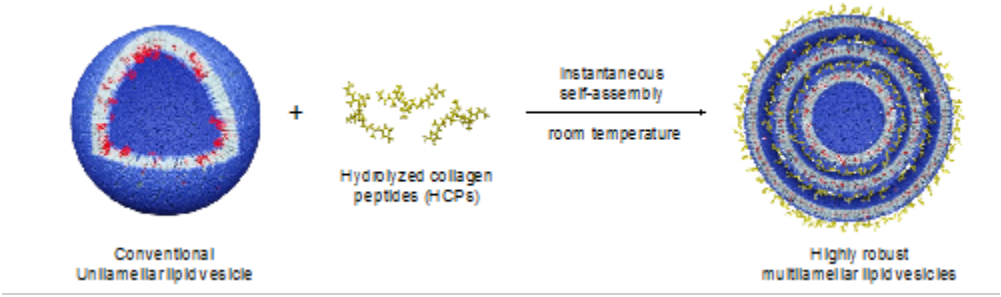

Figure 1. Schematic illustration of the electrostatically driven assembly of LUVs into structurally robust MLVs under ambient conditions. The transformation occurs through simple mixing at room temperature, without the need for external energy input.

2. Materials and Methods

2.1. Materials. HCP (~ 1.57 kDa) and DOTAP were obtained from Italgelatine SpA and Avanti Polar Lipid, Inc., respectively. ATRL and esterase were obtained from Sigma-Aldrich and human dermal fibroblast cell line (HDF) from ATCC. Cell culture reagents (DMEM, FBS, antibiotics, TrypLE) were from GIBCO. EpiDerm™ EPI-200 skin models were obtained from MatTek Corporation.

2.2.Lipid nanovesicle preparation. DOTAP and ATRL were dissolved in chloroform, dried, and vacuumed for 16 h. The film was hydrated with water at 37°C for 2 h. Vesicles were extruded through a 0.1 μm polycarbonate membrane to prepare LUVs. To form MLVs, dialyzed HCP was mixed with LUVs (1:1 v/v) and incubated at 25°C for 10 min to form R-MCLVs. Size was measured using dynamic light scattering (DLS, ELSZ-1000, Otsuka Electronics).

2.3. Characterization. Vesicles were applied to a lacey grid, vitrified in liquid ethane, and imaged using a 300 kV cryo-TEM (JEM-3011 HR, JEOL Ltd.). Small-angle X-ray Scattering (SAXS) was conducted at the Pohang Accelerator Lab with a 0.734 Å X-ray source. Scattering profiles were used to calculate interlamellar spacing ($2\pi/q$). ATRL stability in MLVs was tested by reverse-phase high-performance liquid chromatography (RP-HPLC, 1260 Infinity, Agilent Technologies) using 100% methanol on a C18 column (SunFireTM C18 5 μm) at 1 mL/min for 30 min. For retinol release test, ATRL-loaded vesicles were dialyzed in ethanol/PBS (1:1) at 37°C. Samples were collected over time and analyzed by HPLC. For endosomal escape, MLVs were incubated in citrate buffer with esterase, and ATRL release was measured by UV absorbance at 352 nm.

2.4. Biological evaluation. HDF cells were cultured in 6-well plates using fibroblast basal media supplemented with 10 vol% FBS and 1 vol% penicillin-streptomycin. The cells

were treated with various formulations for 6 h. HDF cells on coverslips were treated with vesicles (10 μg/mL) for 2 h, fixed with paraformaldehyde, stained with Hoechst 33342, and imaged using a spinning disk confocal microscope (Olympus BX51WI). For cytotoxicity test, cells in 96-well plates were treated with LUVs or MLVs (0.001–100 μg/mL) for 24 h. Cell viability was assessed using CCK assay by measuring absorbance at 450 nm. EpiDerm™ skin models were treated topically with samples and incubated for 12 h. After rinsing and trypsinization, cells were dissociated and collected for analysis. Total RNA was extracted and quantified. Relative gene expression (COL1A1 and MMP-1) was measured CFX96 Real-Time System Reverse-Transcription quantitative PCR (RT-qPCR, BIO-RAD, Hercules, CA, USA), normalized to the housekeeping gene 36B4, and expressed as fold change vs. control.

3. Results and Discussion

3.1. Efficient encapsulation of retinol in multilamellar lipid vesicles via collagen-induced structural transformation.

ATRL-loaded HCP-DOTAP MLVs were fabricated through a sequential two-step process. Initially, DOTAP and ATRL were co-dissolved in chloroform at a 9:1 weight ratio, forming a uniform thin lipid film upon solvent evaporation. This film was hydrated with deionized water at 37°C, followed by extrusion through a 0.1 μm polycarbonate membrane to generate ATRL-loaded LUVs. These LUVs were subsequently combined with HCPs to yield MLVs through a spontaneous structuring process. DLS measurements indicated that the mean diameter of the ATRL-loaded LUVs was 155 ± 4.7 nm, slightly smaller than that of unloaded LUVs (161 ± 2.6 nm). This slight reduction suggests that ATRL incorporation does not significantly perturb the vesicle size. Notably, the DOTAP-to-ATRL molar ratio was approximately 3.7, and the ATRL loading efficiency reached an exceptionally high value of 97.6%. This efficiency seems to be attributed to ATRL's hydrophobic character and its elongated molecular geometry, which likely promotes stable intercalation into the lipid bilayer.

To optimize the structural conversion into multilamellar architectures, MLVs were prepared by varying the HCP-to-lipid weight ratio from 0 to 5 (Figure 2a). Across all tested ratios, the resulting MLVs maintained particle sizes comparable to their LUV counterparts, with a slight reduction observed at the ratio of 2 (142.9 ± 5.4 nm) (Figure 2b). Despite the relatively unchanged hydrodynamic diameter, zeta-potential values progressively decreased with increasing HCP content, from 52.9 ± 0.6 mV for LUVs (without HCPs) to 17.9 ± 1.4 mV at the ratio of 5, indicating a significant surface charge neutralization upon HCP complexation. This gradual reduction in zeta-potential is consistent with previous reports on multilamellar complexation involving DOTAP and negatively charged biomolecules such as DNA or proteins, wherein vesicular transformation is typically accompanied by surface charge masking and internal structural rearrangement (Radler et al., 1997; Koo et al., 2021a). Among the formulations tested, MLVs prepared at the HCP-to-lipid weight ratio of 2 were selected for further studies due to their favorable physicochemical properties, including optimal particle size and intermediate zeta-potential values that enhance colloidal stability and support skin delivery applications.

Importantly, ATRL loading efficiency in MLVs remained high at 97.5%, closely matching that of the initial LUVs. This observation indicates that the multilamellar assembly process does not compromise drug encapsulation. The consistent particle size, in conjunction with the pronounced decrease in zeta-potential, implies strong interactions between HCPs and the LUV surface. However, the observed reduction in particle size upon MLV formation cannot be solely attributed to surface adsorption of HCPs, suggesting that a more complex mechanism, potentially involving membrane compaction or inter-vesicle fusion, may contribute to the generation of densely packed multilamellar structures.

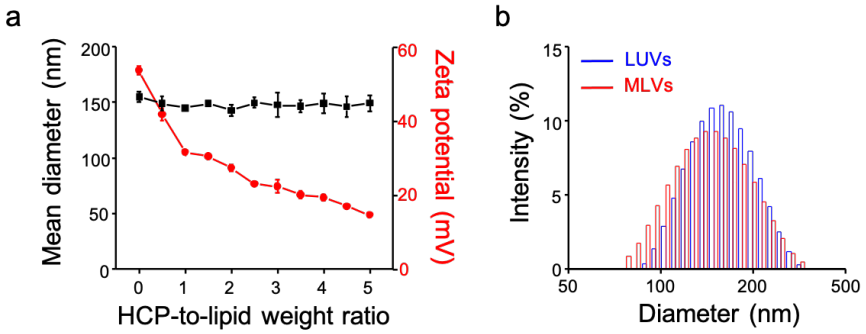

Figure 2. (a) Hydrodynamic diameter and zeta potential of lipid vesicles at varying HCP-to-LUV weight ratios. Data are presented as mean ± standard deviation (black squares: mean diameter; red circles: zeta potential). (b) Size distribution profiles of LUVs (blue) and MLVs (red) obtained by DLS.

3.2. Structural characterization of retinol-loaded multilamellar lipid vesicles

The morphological features of retinol-loaded LUVs and their corresponding MLVs were investigated using cryogenic transmission electron microscopy (cryo-TEM). As shown in Figure 3a, LUVs displayed well-defined unilamellar structures, characterized by a single lipid bilayer. While no significant changes in vesicle diameter were observed upon ATRL incorporation, a notable increase in membrane thickness was detected from 4.9 ± 1.3 nm to 5.2 ± 1.4 nm. This finding suggests that ATRL, due to its hydrophobic and elongated molecular structure, is likely embedded within the hydrophobic core of the membrane, effectively expanding the vertical dimension of the non-polar domain. It is important to note that while particle size is primarily influenced by mechanical processing such as extrusion, membrane thickness is governed by the intrinsic molecular arrangement within the lipid bilayer. Interestingly, even with a high concentration of ATRL present in the LUVs, the formation of multilamellar assemblies was not inhibited (Figure 3b). Upon complexation with HCPs, the membrane thickness further increased to 6.9 ± 1.2 nm. These increases in bilayer thickness are in agreement with previously reported results on similar multilamellar vesicle systems (Koo et al., 2021a; Koo et al., 2023), where HCP-induced vesicle restructuring was associated with increased membrane condensation and interbilayer interactions. One proposed mechanism is the formation of ionic interactions, such as salt bridges, between adjacent membranes and HCPs, which may facilitate tighter lateral lipid packing while introducing slight bilayer disorder. Though the precise molecular mechanism remains to be fully elucidated, the physical changes observed indicate strong HCP-lipid interactions. Cryo-TEM analysis also revealed consistent bilayer stacking in MLVs regardless of ATRL loading, with the average number of bilayers per vesicle measured as 2.5 ± 0.9 and 2.6 ± 1.1 for MLVs without and with ATRL loading. Importantly, no evidence of vesicle rupture or membrane fragmentation was observed, indicating that the HCP-mediated assembly process promotes membrane reorganization without compromising bilayer integrity. This reinforces the conclusion that HCP facilitates a vesicle-to-vesicle structural transformation into stable multilamellar configurations, rather than disrupting the lipid assembly.

To further confirm the internal architecture of the vesicles, SAXS was employed on both LUVs and MLVs. The SAXS profile of MLVs exhibited sharp Bragg peaks at q-values of 0.056, 0.112, and 0.171 $Å^{-1}$ (Figure 3c), with peak ratios corresponding to 1:2:3. This pattern is characteristic of a well-ordered lamellar phase, supporting the multilamellar structural formation and aligning with previous findings (Radler et al., 1997). Calculated interlamellar spacing (d_lamellar) for all multilamellar samples, regardless of ATRL presence, was consistently measured at 11.0 nm. This value reflects the combined thickness of the lipid bilayer and the intervening aqueous layer containing HCPs. Additional analysis integrating cryo-

TEM and SAXS data enabled estimation of the aqueous interstitial space, yielding values of 5.1 nm for MCLVs and 4.7 nm for MLVs (Figure 2d). These dimensions are sufficient to accommodate HCPs between bilayers, supporting their successful incorporation.

Taken together, the results indicate that ATRL loading does not interfere with multilamellar structure formation. The preserved interlamellar spacing and similar bilayer numbers in MLVs suggest that the structural integrity of the vesicle is maintained despite ATRL incorporation. These results suggest the robustness of the HCP-DOTAP multilamellar system and its potential utility in delivering hydrophobic therapeutics such as ATRL through a stable and tunable vesicular architecture.

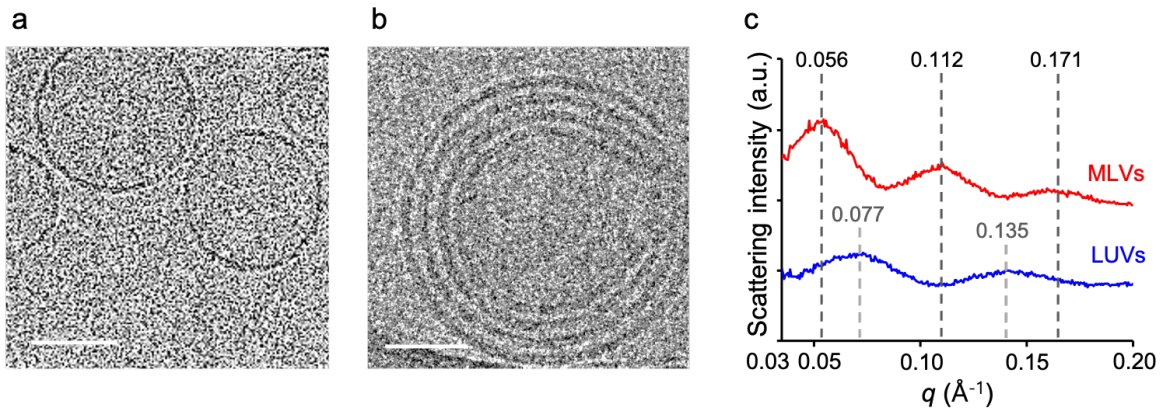

Figure 3. Cryo-TEM images of LUVs (a) and MLVs (b). Scale bar = 100 nm (a) and 50 nm (b). SAXS profiles of LUVs and MLVs.

3.3. Retinol stability within multilamellar lipid vesicles

The long-term chemical stability of ATRL encapsulated within LUVs and MLVs was evaluated using RP-HPLC. Stability profiles were monitored over a period of 90 days at 4°C (refrigerated), 25°C (ambient), and 37°C (physiological). At all tested conditions, ATRL encapsulated in LUVs exhibited pronounced degradation, with substantial reductions in peak intensity observed even during the early phase of storage. In contrast, ATRL encapsulated in MLVs demonstrated remarkable resistance to degradation, with retention rates remaining largely unchanged at 4°C and 25°C throughout the testing period. Specifically, LUVs showed approximately 40% loss of ATRL within the first two weeks at both 4°C and 25°C, with degradation plateauing after 30 days (Figures 4a and 4b). At 37°C, ATRL degradation in LUVs occurred even more rapidly, falling below 30% of the initial concentration within 7 days. This pronounced instability is attributed to the proximity of 37°C to the phase transition temperature of DOTAP (41.3°C), which likely compromises the vesicular membrane structure and enhances lipid bilayer fluidity, thereby accelerating chemical breakdown (Figure 4c). In contrast, MLVs maintained ATRL integrity at both 4°C and 25°C; no significant degradation was observed over the entire 90-day period. HPLC chromatograms further confirmed this enhanced stability: LUVs showed a reduction in the primary ATRL peak along with the emergence of secondary degradation peaks (data not shown), while MLVs retained sharp and singular ATRL peaks without detectable byproducts. These results suggest that the multilamellar architecture, characterized by densely packed and ordered bilayers, creates a more rigid and less permeable environment that inhibits molecular diffusion and retinol exposure to external degradative factors. The improved retention of ATRL in MLVs is likely attributed to two primary mechanisms: (1) the reduced lipid exchange across layers, which minimizes interfacial exposure, and (2) the suppression of bilayer fluidity, particularly at temperatures near or above the melting temperature of lipids. Together, these structural attributes of MLVs

provide a favorable microenvironment for preserving labile hydrophobic molecules such as retinol, especially in formulations requiring prolonged shelf life (Koo et al., 2023).

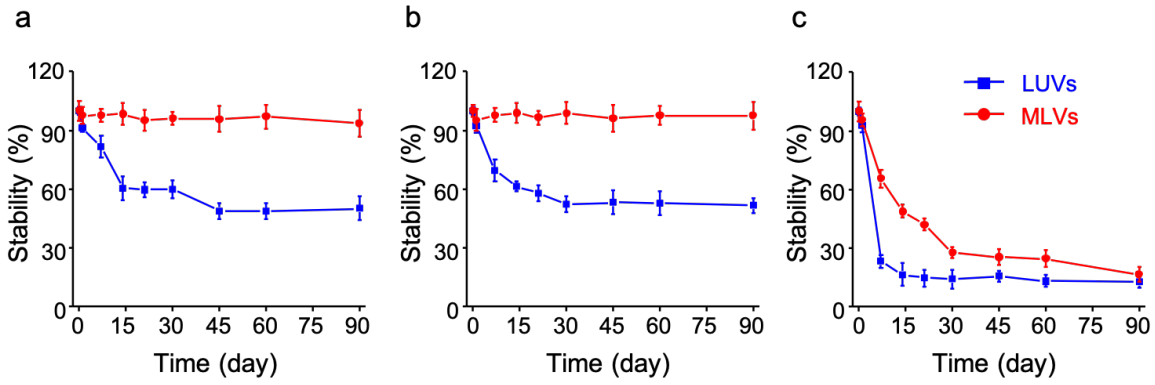

Figure 4. Chemical stability of ATRL encapsulated within LUVs and MLVs incubated at 4°C (a), 25°C (b), and 37°C (c) for 90 days (n = 5 and average ± standard deviation).

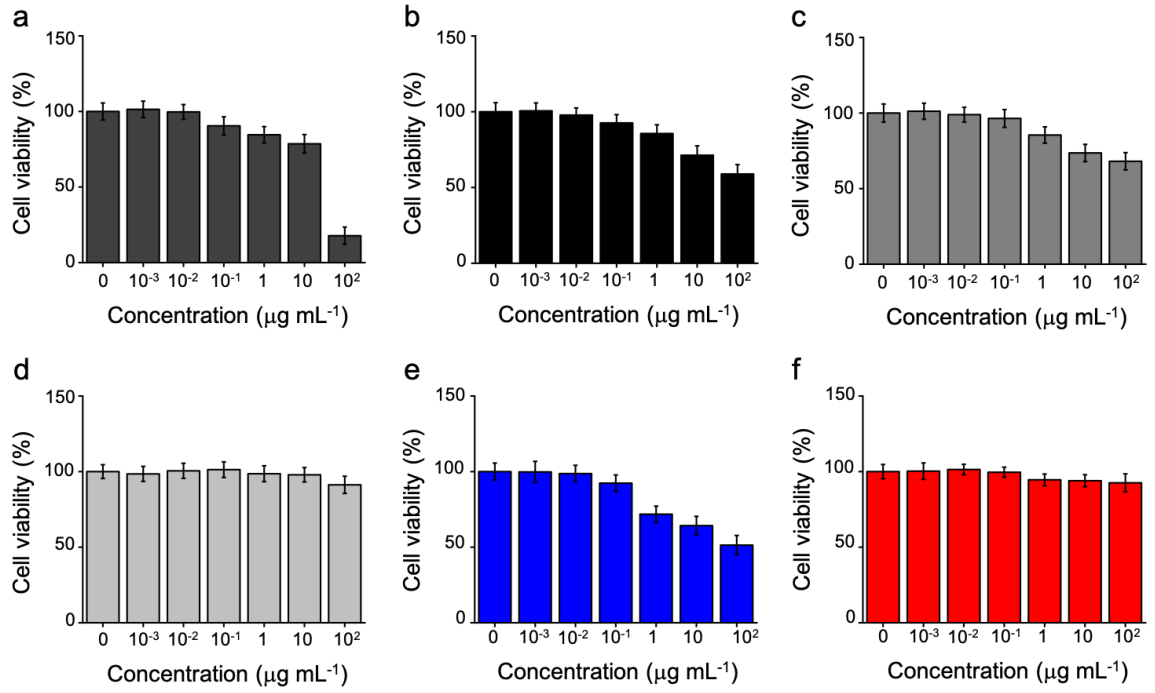

Figure 5. Cell cytotoxicity of various formulations by CCK-8 assay. HDFa cells were treated with SDS (a), free ATRL (b), blank LUVs (c), blank MLVs (d), LUVs (e), and MLVs (f). Data are presented as mean ± standard deviation (n = 5).

3.4. Multilamellar vesicles attenuate atrl-induced cytotoxicity

The cytotoxic effects of various formulations, including free ATRL, blank nanocarriers, and ATRL-loaded nanocarriers (LUVs and MLVs), on human dermal fibroblasts (HDFa) were quantitatively assessed using the CCK-8 assay (Figure 5). Solubilized ATRL, delivered in ethanol as a free active ingredient, induced a significant and dose-dependent reduction in cell viability, decreasing from 82.8 ± 5.8% to 60.2 ± 6.2% across a concentration range of 1 to 10 μg/mL ($p < 0.0001$). This trend indicates the intrinsic cytotoxicity of ATRL at pharmacologically relevant doses, likely due to its pro-oxidant and membrane-disruptive properties.

Interestingly, the blank LUVs, composed of cationic DOTAP lipids without ATRL loading, also exhibited notable cytotoxicity, even in the absence of an active ingredient. This observation is consistent with previous findings that cationic liposomes can destabilize cell membranes through strong electrostatic interactions with negatively charged phospholipid bilayers and surface glycoproteins on mammalian cells. Upon ATRL loading, the cytotoxicity of the liposomes further intensified, as reflected in the lower cell viability observed with LUVs compared to blank LUVs. This enhanced toxicity is likely a cumulative result of both the membrane-disrupting nature of the cationic lipid and the bioactivity of encapsulated ATRL. In contrast, both blank MCLVs and ATRL-loaded MLVs demonstrated markedly lower cytotoxic effects, maintaining cell viability above a critical threshold and showing minimal statistical difference between each other. These results suggest that the multilamellar architecture plays a protective role by decreasing the total number of particles and reducing the exposed surface area that can interact with the cellular membrane (Figure 6). Consequently, this structural characteristic is hypothesized to mitigate the cytotoxic impact of both the lipid components and the encapsulated drug, potentially by limiting cellular uptake or slowing drug release at the membrane interface. This interpretation is supported by previous work (Wei et al., 2015), which explored the influence of vesicle lamellarity on cellular responses, particularly in relation to membrane compatibility and particle-cell interactions.

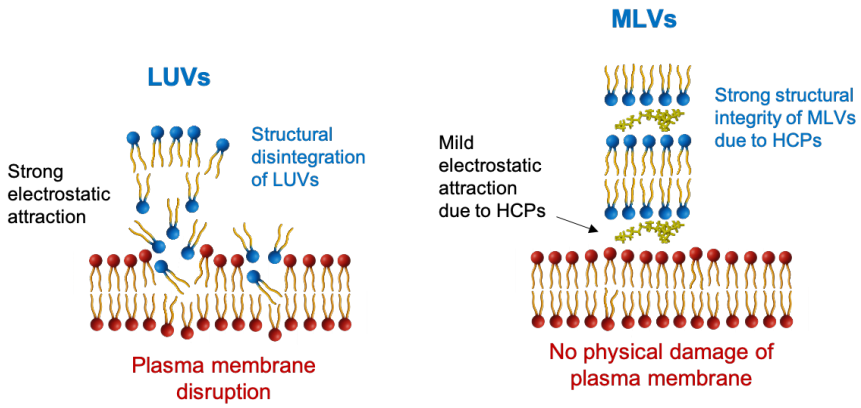

Figure 6. Schematic illustration of plasma membrane disruption induced by strong electrostatic interactions between positively charged LUVs and the negatively charged cell membrane. In contrast, HCPs on the surface of MLVs reduce surface charge density, thereby mitigating cytotoxicity associated with non-specific membrane disruption. Additionally, due to their multilamellar structure, the number of MLVs is significantly lower than that of LUVs at the same lipid mass concentration.

3.5. Controlled release and structural stability of ATRL-loaded multilamellar vesicles

The release kinetics of ATRL from LUVs and MLVs were evaluated using a dialysis method, wherein vesicles were enclosed in a membrane with a molecular weight cut-off (MWCO) much higher than that of ATRL and immersed in 50% ethanol at 37°C (Figure 7a). This ethanol-based medium was selected to ensure sufficient solubility of the hydrophobic ATRL and maintain sink conditions. MLVs exhibited a significantly slower release than LUVs within the initial 2 hours, followed by a gradual, sustained release over 12 hours. After 4 hours, cumulative ATRL release from LUVs reached 63.8%, while MLVs released only 23.7%, indicating improved drug retention by the multilamellar structure. To determine whether the high ethanol concentration affected vesicle integrity, LUVs and MLVs were incubated in 50% ethanol and analyzed via DLS and cryo-TEM. LUVs showed a split size distribution and formed micron-scale aggregates, suggesting ethanol-induced disruption (Figure 7b). In contrast, MLVs retained a single, stable size distribution (198.9 ± 3.4 nm), with a slight size increase likely due to swelling (Figure 7c). Cryo-TEM confirmed that LUVs appeared collapsed and aggregated (Figure 7d), while MLVs preserved their multilamellar structure (Figure 7e).

Further release studies were performed in PBS (pH 7.4) and sodium citrate buffer (pH 5.0) to simulate endolysosomal conditions (Figure 7f). MLVs showed minimal ATRL release under both conditions over 24 h, supporting their pH stability. However, in citrate buffer (pH 5.0) containing 0.5 U/mL esterase and 140 mM NaCl, ATRL release was significantly increased, suggesting that enzymatic cleavage of lipid ester bonds disrupted the lamellar structure. These results indicate the potential of R-MCLVs for controlled and stimuli-responsive drug delivery.

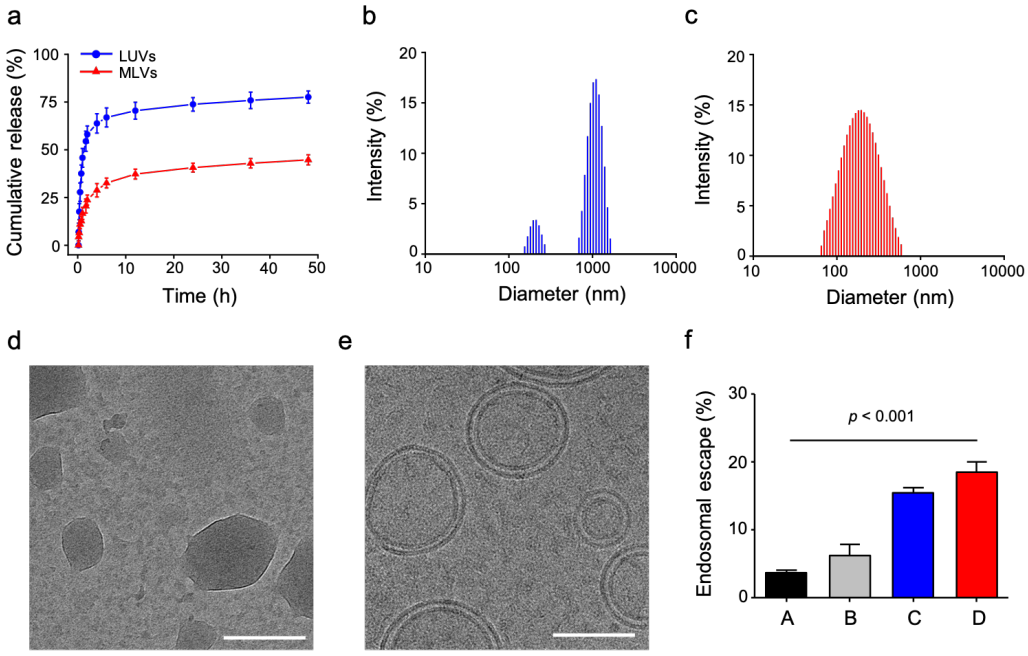

Figure 7. (a) Cumulative release of ATRL from LUVs and MLVs under sink conditions. Size distributions of LUVs (b) and MLVs (c) incubated in a 50% ethanol solution. After incubating LUVs and MLVs (1 mg/mL, 1 mL) in 50% ethanol (10 mL) for 8 h, DLS analysis was conducted with adjusted refractive index (1.347), viscosity (0.9947), and dielectric constant (5.17). Cryo-TEM images of LUVs (d) and MLVs (e) incubated in a 50% ethanol solution. Scale bars = 200 nm. (f) Percentage of the release rate of ATRL from MLVs for 24 h under various conditions (n = 5 and average ± standard deviation): A, PBS (pH 7.4); B, sodium citrate (pH 5); C, esterase in sodium citrate (pH 5); and D, esterase in sodium citrate with 140 mM NaCl (pH 5).

3.5. Influence of Vesicle Structure on Cellular Uptake Efficiency

To investigate how vesicle structure affects cellular internalization, the uptake of coumarin 6-labeled LUVs and MLVs by HDFa was visualized using spinning disk confocal microscopy (Figure 8a). Free coumarin 6, initially solubilized in ethanol at a concentration of 5 mg/mL and subsequently diluted 100-fold in PBS, formed aggregates and underwent fluorescence quenching, making it unsuitable for evaluating passive diffusion. In contrast, both LUVs and MLVs effectively delivered coumarin 6 into HDFa cells, as evidenced by strong green fluorescence localized predominantly in the cytoplasmic region, alongside nuclear staining with Hoechst 33342. Quantitative analysis revealed that cells treated with LUVs exhibited significantly higher intracellular fluorescence intensity than those treated with MLVs, showing a 1.3-fold increase in signal per cell ($p < 0.001$) (Figure 8b). This difference is likely due to the distinct structural properties of the vesicles: LUVs, being unilamellar, exist in greater particle numbers at a given lipid concentration compared to their multilamellar counterparts. As a result, even when the same overall lipid dose is administered, the number of particles, and thus the total number of uptake events per cell, is considerably higher for LUVs. These res-

ults suggest that vesicle architecture plays a key role in modulating the extent of cellular uptake, independent of lipid content alone.

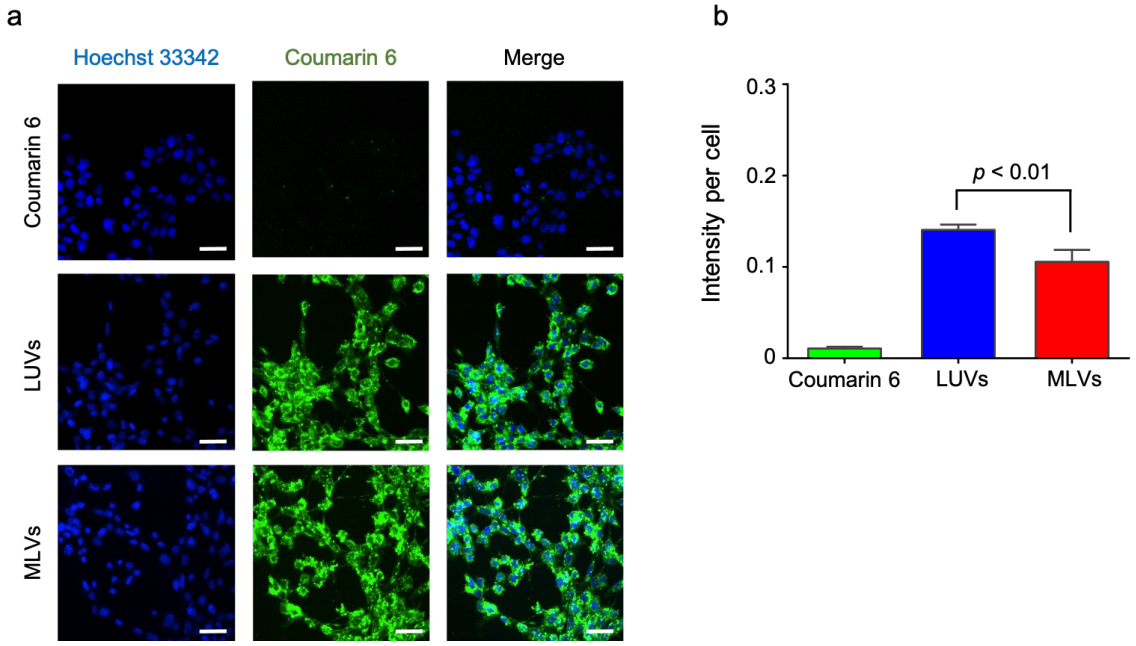

Figure 8. Confocal microscopy images (a) and green/blue fluorescence intensity per cell (b) showing the internalization of coumarin 6-loaded LUVs and MLVs (green) by HDFa cells. Cell nuclei were counterstained with Hoechst 33342 (blue). Scale bar = 20 µm.

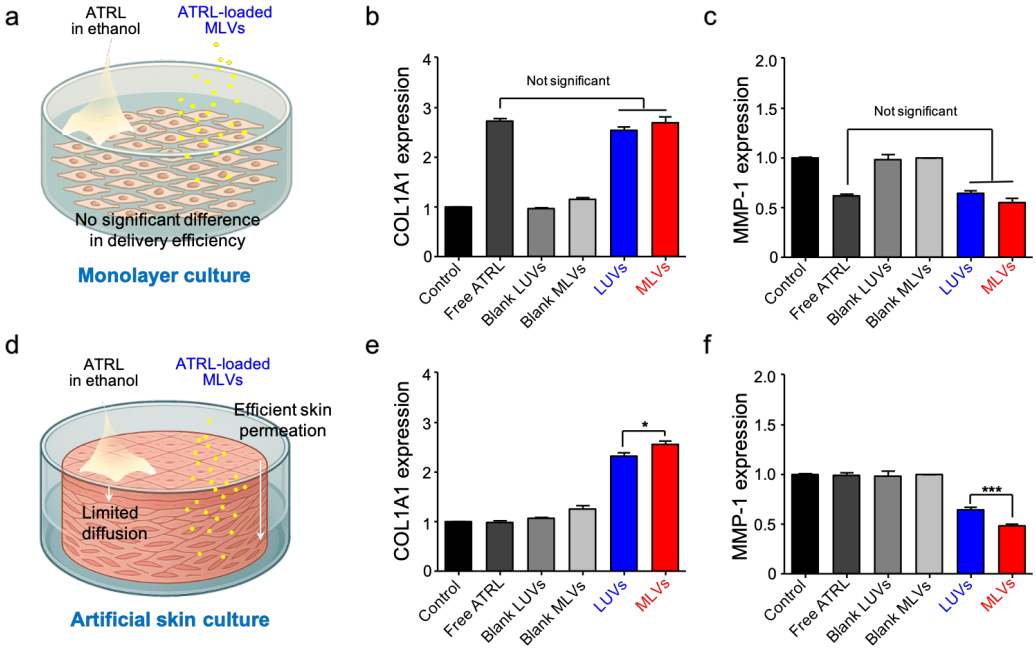

Figure 9. (a) Schematic illustration of the treatment procedure on monolayer HDFa cell cultures. Gene expression levels of COL1A1 (b) and MMP-1 (c) after treatment with free ATRL, blank LUVs and MLVs, LUVs, and MLVs. (d) Schematic illustration of the treatment procedure on a 3D human skin model. Gene expression levels of COL1A1 (e) and MMP-1 (f) following treatment with the same formulations. Results are expressed as fold changes relative to the vehicle control (n = 5, mean ± standard deviation).

3.6. Therapeutic effects of LUVs and MLVs on collagen and MMP expression

The therapeutic efficacy of R-MCLVs was assessed by analyzing COL1A1 and MMP-1 gene expression in HDFs (Figure 9a). Cells were treated for six hours with free ATRL, blank LUVs or MLVs, or ATRL-loaded LUVs or MLVs, followed by RT-qPCR. Free ATRL and both ATRL-loaded nanocarriers significantly upregulated COL1A1 expression compared to vehicle and blank controls, which showed no effect ($p > 0.05$) (Figure 9b). COL1A1 expression increased dose-dependently across ATRL concentrations from 0.25 to 5 nM, with no significant differences between free and encapsulated forms. MMP-1 expression was reduced by ~50% with free ATRL, LUVs, and MLVs, again in a concentration-dependent manner (Figure 9c). No significant effects were observed with free HCP or blank carriers. The reduction in MMP-1 expression, a key mediator of collagen degradation, may contribute synergistically to enhanced collagen synthesis. Figure 9d shows further evaluation using a 3D reconstructed human skin model (EpiDerm™). The results showed that LUVs and MLVs increased collagen gene expression (Figure 9e), whereas free ATRL had no significant effect ($p > 0.05$), likely due to poor skin penetration (Ahn and Nam, 2024). In contrast, LUVs and MLVs penetrated the epidermis effectively, with MLVs exhibiting lower toxicity and slightly higher collagen induction ($p < 0.05$) due to their greater stability. Both nanocarriers also reduced MMP expression, with MLVs being significantly more effective than LUVs ($p < 0.001$), suggesting stronger anti-degradative activity within the skin model (Figure 9f).

4. Conclusion

In this study, we developed robust ATRL-loaded multilamellar lipid vesicles as an efficient nanocarrier system for stabilization and cutaneous delivery of ATRL. The multilamellar architecture of MLVs was confirmed through cryo-TEM and SAXS analyses. These vesicles exhibited a remarkably high ATRL encapsulation efficiency of 97.5% and retained their structural integrity for up to 90 days under storage conditions. Biocompatibility studies using HDFa cells revealed that ATRL-encapsulated MLVs maintained high cell viability, exceeding 90%. At the molecular level, treatment with MLVs significantly upregulated the expression of collagen genes, while effectively downregulating the protein expression of matrix metalloproteinases, indicating their potential to promote collagen synthesis and preserve the extracellular matrix. When applied to a 3D human skin model, MLVs outperformed free ATRL in enhancing biological responses, underscoring their efficacy in cutaneous applications. Collectively, these results highlight multilamellar lipid vesicles as a promising platform for the stable and effective topical delivery of ATRL.

5. Acknowledgments

This work was supported by the National Research Foundation of Korea (NRF) grant funded by the Korea government (MSIT) (RS-2025-00516761). Experiments at PLS-II were supported in part by MSIP and POSTECH (Pohang, Republic of Korea).

6. References

Ahn and Nam. Assessing Barrier Function in Psoriasis and Cornification Models of Artificial Skin Using Non-Invasive Impedance Spectroscopy. *Adv Sci.* 2024 Sep;11(34):e2400111.

Koo et al. Protein-induced metamorphosis of unilamellar lipid vesicles to multilamellar hybrid vesicles. *J Control Release.* 2021 Mar 10;331:187-197.

Koo BI et al. Highly Robust Multilamellar Lipid Vesicles Generated through Intervesicular Self-Assembly Mediated by Hydrolyzed Collagen Peptides. *Biomacromolecules.* 2023 Jul 10;24(7):3043-3050.

Rahman et al. Multilayered collagen-lipid hybrid nanovesicles for retinol stabilization and efficient skin delivery. *Int J Pharm.* 2024 Aug 15;661:124409.

Wei et al. Cationic nanocarriers induce cell necrosis through impairment of Na(+)/K(+)-ATPase and cause subsequent inflammatory response. *Cell Res.* 2015 Feb;25(2):237-53.